Observations of Land Surface Passive Polarimetry With the WindSat Instrument

Parag S. Narvekar, Thomas J. Jackson, *Fellow, IEEE*, Rajat Bindlish, *Senior Member, IEEE*, Li Li, *Senior Member, IEEE*, Georg Heygster, *Member, IEEE*, and Peter Gaiser, *Senior Member, IEEE*

***Abstract*—WindSat provides an opportunity to explore the passive microwave polarimetric signatures of land surfaces. In order to accommodate the large sensor footprint, large homogeneous regions with unique features were used. These included forest, rangeland, desert, and agricultural conditions. WindSat observations at horizontal and vertical polarizations over land surfaces were found to be well calibrated and consistent with other passive microwave sensors. Isotropic regions (e.g., Amazon rainforest) had no polarimetric response at all azimuth angles. Results showed that land surfaces with aligned features (topography or row structured vegetation) produced systematic variations in the third and fourth Stokes parameters. These responses were found to be in good agreement with previous sea surface studies. Analysis of the temporal trends of the variation in polarimetric measurements for a specific azimuth angle could be attributed to the crop growth cycle in the agricultural region. Further analyses will seek to isolate specific features that could be used in applications such as soil moisture retrieval.**

***Index Terms*—Microwave radiometry, polarimetric, soils, vegetation, WindSat.**

I. Introduction

PASSIVE microwave remote sensing has been shown to be a valuable source of information for land applications such as large-scale soil-moisture retrieval. A limitation of these retrievals is that there are often more parameters that need to be determined than there are independent observations. These parameters include multiple scales of roughness and potentially several vegetation characteristics. One way to deal with this issue is by using ancillary data sources. However, this can be challenging, and a retrieval based upon a single sensor package may be more efficient.

Traditional spaceborne microwave radiometers have provided multifrequency dual-polarization data. The WindSat instrument provides the first spaceborne fully polarimetric microwave measurements of the Earth's emission. The primary objective of the WindSat satellite is to provide information for sea surface wind vector (speed and direction) retrievals. The data are also acquired over land surfaces and thus offer a new opportunity to investigate the possibility of introducing fully polarimetric measurements in land surface applications. WindSat measures the vertical (ν) and horizontal (h) polarized brightness temperature (T_B) at 6.8 and 23.8 GHz. In addition to ν and h, it measures brightness temperature at -45°, $+45^\circ$, and right and left circular polarizations at 10.7, 18.7, and 37 GHz [1]. Data are provided in the form of the modified Stokes vector, which defines the polarimetric state of an electromagnetic wave and can be written as [1], [2]

$$I = \begin{bmatrix} T_\nu \\ T_h \\ T_{-45} - T_{45} \\ T_{lc} - T_{rc} \end{bmatrix} = \begin{bmatrix} T_\nu \\ T_h \\ U \\ V \end{bmatrix}. \quad (1)$$

The first two parameters of the modified Stokes vector are the vertical and horizontal polarized brightness temperatures, T_ν and T_h. The third Stokes parameter (U) is the difference between the brightness temperature of the -45° and $+45^\circ$ channels, and the fourth Stokes parameter (V) provides the difference between the left- and right-handed circularly polarized T_B [1].

The brightness temperatures T_ν and T_h are primarily functions of surface temperature and dielectric constant. As a result, T_B is inversely correlated to soil moisture and positively correlated to soil temperature [3]. In addition, the modulation of brightness temperature may also depend upon the Earth's surface geometric properties [4], [5]. It is difficult to estimate the modulation in brightness temperature due to land surface geometric structure using only T_ν and T_h, for the regions where the expectancy of temporal variations in soil moisture and surface temperature is higher. The polarimetric signature U and V over the sea surface has been shown to be primarily a function of surface structure. However, a thorough analysis for land surfaces has not been conducted.

Our analysis focuses on the WindSat observations over several large and homogeneous regions for an extended period. These include azimuthal isotropic and systematically structured anisotropic areas. The U and V parameter responses over the isotropic areas are expected to be 0 K, and for the structured regions, we expect nonzero U and V responses. This paper demonstrates the presence of a land surface structure signature in the polarimetric U and V measurements even at the scale of a satellite footprint. It is possible that the information present in

Manuscript received May 5, 2006; revised July 25, 2006.

P. S. Narvekar, T. J. Jackson, and R. Bindlish are with the Hydrology and Remote Sensing Laboratory, U.S. Department of Agriculture, Beltsville, MD 20705 USA.

L. Li and P. Gaiser are with the Naval Research Laboratory, Washington, DC 20375, USA.

G. Heygster is with the Institute of Environmental Physics, University of Bremen, D-28334 Bremen, Germany.

Color versions of one or more of the figures in this paper are available online at http://ieeexplore.ieee.org.

Digital Object Identifier 10.1109/TGRS.2006.886963

these parameters may be helpful in improving the retrieval of land surface geophysical parameters.

II. Polarimetric Variables and Expected Responses

Passive microwave polarimetry has been extensively studied for sea surface applications, but very little has been investigated over land. The launch of WindSat has provided an opportunity to study the polarimetric measurements of the Earth's emission from space. In this section, a basis for WindSat polarimetry of land surfaces is developed from theoretical models [6], previously conducted airborne passive polarimetric studies over ocean surfaces [7], [8], and ground-based studies over land surfaces [9]–[11].

For sea surfaces, the response of the U and V parameters is primarily dependent on sea surface roughness, which is a function of the wind vector [7]. A two-scale sea surface roughness approach has been found to yield better results in the wind vector retrievals [7]. The "two-scale" refers to two levels of roughness, one from large waves on the order of meters and the other from small capillary waves on the order of centimeters, which lie on top of large-scale waves [7]. These studies also showed the dependence of U and V on the azimuth look angle of a radiometer. In that study, all Stokes parameters were represented as second harmonic sine functions of the relative azimuth angle $\varphi_{\rm relative}$, as presented in (2)–(5). The relative azimuth angle is the difference between the wind direction $\varphi_{\rm wind}$ and the radiometer azimuth angle $\varphi_{\rm rad}$, given as $\varphi_{\rm relative} = \varphi_{\rm wind} - \varphi_{\rm rad}$ [4]

$$T_\nu \approx T_{\nu_0} + T_{\nu_1} \cos\varphi_{\rm relative} + T_{\nu_2} \cos 2\varphi_{\rm relative} \quad (2)$$

$$T_h \approx T_{h_0} + T_{h_1} \cos\varphi_{\rm relative} + T_{h_2} \cos 2\varphi_{\rm relative} \quad (3)$$

$$U \approx U_1 \sin\varphi_{\rm relative} + U_2 \sin 2\varphi_{\rm relative} \quad (4)$$

$$V \approx V_1 \sin\varphi_{\rm relative} + V_2 \sin 2\varphi_{\rm relative}. \quad (5)$$

In these relations, the first harmonic primarily accounts for up-wind and down-wind asymmetry, and the second harmonic accounts for up-wind and cross-wind asymmetry [7]. The up-wind, down-wind, and cross-wind (only the gravity waves) can be expressed in terms of the slopes of these waves in the leeward, windward, and in the direction perpendicular to leeward or windward, respectively. Usually, the polarimetric signal produced by gravity waves gets modified by small-scale capillary waves superimposed on these waves. The harmonic dependence of U and V on the orientation of the sea waves results in negative or positive values of these parameters.

In translating the results described above to the land surface, the orientation of the topographic slopes at different scales, ranging from kilometers to centimeters, is expected to produce responses in the U and V parameters. In this paper, we have symbolized the orientation of the land surface structure by $\varphi_{\rm orient}$, which is equivalent to $\varphi_{\rm wind}$ in terms of sea surface.

For land surfaces, Tsang [6] derived theoretical expressions for all Stokes parameters. In that study, the nonzero third and fourth Stokes parameters were considered a result of land surface roughness and were also expressed as a function of the azimuth angle. Nghiem *et al.* [11] conducted a ground-based experiment and showed the azimuthal dependence of brightness temperature on soil surface structure. In that study, a periodic soil surface was created, and measurements were made for the h, ν, and 45° planes at different azimuth angles. The 45° T_B along with the difference between h and ν was used to calculate the third Stokes parameter.

In the presence of vegetation, the Stokes parameters are expected to depend primarily on biomass structure. The few available ground-based experimental studies that have been conducted have shown the dependence of polarimetric measurements on agricultural field rows and crop structure [9], [10]. In these studies, measurements over an agricultural field were acquired during different stages of crop growth. In the absence of vegetation, a plowed soil surface produces a polarimetric signal, which decreases as rainfall smoothes the surface. When there was vegetation, the biomass structure produced a polarimetric signal that is likely to be a function of crop height and field row orientation. These studies also showed that the V signal is 180° out of phase with U, which also agrees with the sea surface studies. The scale of V variation was found to be 1/4th of U, which was also observed for sea surfaces [7], [9]. The physical definition (1) of the V component indicates its dependence on the phase difference between the vertical and horizontal T_B measurements. In the case of a sea surface, the wavelengths of the capillary waves are on the scale of centimeters and may have an impact on V measurements at WindSat frequencies. For land surfaces, we are unaware of any similar phenomena.

In general, land surfaces can be considered as highly variable with different levels of roughness coming from different surface features of the Earth, such as terrain on the scale of kilometers, smaller topographic variation on the scale of meters, roughness at centimeter scales, etc. In the presence of vegetation cover, the primary effect of the vegetation structure is expected in the polarimetric signature. The vegetation structure may be considered as being composed of individual plant or tree structure along with the height or orientation of agricultural field rows, etc.

III. Study Area Descriptions

Further understanding of the passive microwave polarimetric features of land surfaces would benefit from observations of well-known sites. Currently, one source of data is the WindSat sensor. Developing an observation-based analysis using coarse spatial resolution satellite data is challenging for the following reasons.

1) All of the surface and vegetation effects described above can occur individually or at the same time.
2) They can also vary with time (plant growth cycle or soil moisture from precipitation).
3) The azimuth angle changes with each pass.

4) The exact footprint center will rarely ever be the same (pass to pass).
5) Spatial variations will typically occur at the scales much smaller than a WindSat footprint, which means there could be a mixture of conditions.

Our approach to limiting the impact of these issues was to use study sites that:

1) had uniform conditions over a spatial domain larger than a satellite footprint;
2) represent diverse conditions;
3) use areas large enough so that frequent temporal observation were possible for a fixed range of azimuth angles.

As a result, we selected the following four sites.

1) Amazon rainforest in Brazil (Lat: -7.5° to -6.5°; Lon: -66.0° to -65.0°): This area represents a dense vegetation condition that remains invariant throughout the year due to the abundance of rainfall (around 2500 mm annually). It has been used previously [12] as a vicarious calibration hot target because of the consistent long-term behavior of T_ν and T_h. Second, the presence of dense vegetation makes the emission generated in all polarization planes similar, making this area highly isotropic in nature. U and V measurements are expected to be 0 K over an isotropic area. These areas provide an excellent calibration target for U and V measurements.
2) Rangelands in Mongolia (Lat: 45.8° to 46.8°; Lon: 106.1° to 107.5°): This area represents lightly vegetated grassland conditions. Occasional rain events are expected in summer months, and snow may occur in winter (November to January). The study area is well instrumented for *in situ* soil moisture measurements and has been used for validating satellite soil moisture retrievals [13]. Low topographic variability under sparse vegetation provides a homogenous isotropic target for testing U and V responses under varying soil-moisture conditions.
3) Taklamakan Desert in China (Lat: 37.5° to 38.5°; Lon: 82.5° to 83.5°): This area is a cold desert with a highly structured sand surface in the northwest part of China. The presence of large sand dunes makes this area a highly anisotropic target. These large structures, easily seen in Fig. 1(a), are oriented northeast with their slopes facing northwest and southeast. Due to this systematic orientation over an area larger than the footprint of a radiometer, this area facilitates the study of WindSat U and V over the land. This site had been identified as an anisotropic target in [14].
4) Heilongjiang agricultural area in China (Lat: 47.0° to 48.0°; Lon: 125.0° to 126.0°): This area represents agricultural fields with almost all the field rows oriented north–south [Fig. 1(b)]. The main crops grown are corn and soybean. The vegetation is present during summer months. In winter, the region is mainly bare soils with possibility of snow. Features of this site had been analyzed in [14] and [15].

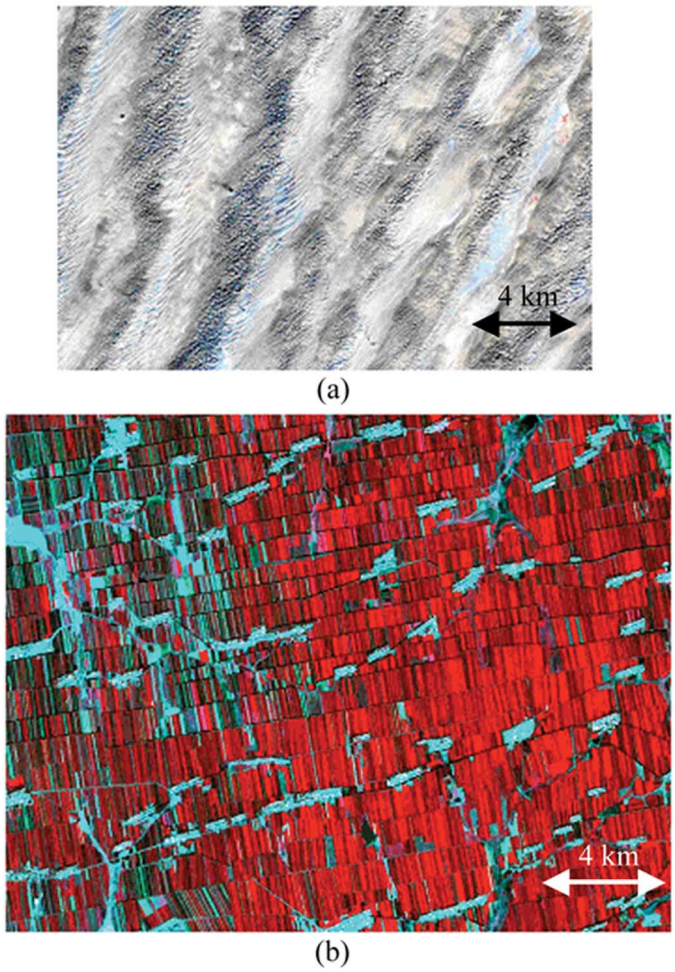

Fig. 1. Advanced Spaceborne Thermal Emission and Reflection Radiometer (ASTER) images over (a) the Taklamakan Desert area in China, acquired on August 25, 2005, and (b) the Heilongjiang agricultural area in China, acquired on August 22, 2005. North is at the top of each image, and the spatial resolution of the data used was 15 m.

IV. WindSat Data

WindSat is the first spaceborne fully polarimetric microwave radiometer. The mission provides risk reduction for an instrument called the Conically Scanned Microwave Imager Sounder that may be part of the National Polar-Orbiting Operational Environmental Satellite System. WindSat was launched on January 6, 2003, into a sun-synchronous orbit with an altitude of 830 km.

For the current investigation, the sensor-data-record version 1.9, available from February 2003 to November 2005, was used. WindSat was in an extended safe mode from February 12–June 17, 2005, and no data were collected during this period. In the microwave remote sensing of the Earth's surface, incidence angle plays a critical role [12]. Studies have shown a dependence of polarimetric measurements on the azimuth angle in addition to the incidence angle [7], [9]. For WindSat, the incidence angle is fixed for each channel (Table I), but azimuth look angle will vary.

Azimuth look geometry involves two components, the scan and azimuth angles. The scan angle $(\varphi_{\rm scan})$ is the radiometer

TABLE I
WINDSAT SENSOR CHARACTERISTICS

Frequency Band in GHz	Polarizations	Earth Incident angle in degrees	Horizontal spatial resolution in kilometers
6.8	*v, h*	53.5	40x60
10.7	*v, h, U, V*	49.9	25x38
18.7	*v, h, U, V*	55.3	16x27
23.8	*v, h*	53.0	12x20
37	*v, h, U, V*	53.0	8x13

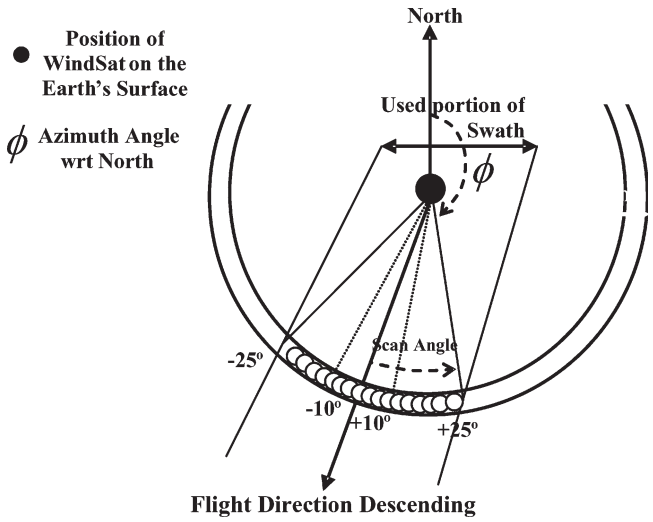

Fig. 2. WindSat simplified data acquisition geometry for a descending orbit. The -25° to $+25^\circ$ shows the selection of radiometer scan angle in forward swath for the entire analysis. The scan angle between -10° and $+10^\circ$ shows the selection for averages of the data on a given date.

look angle with respect to the flight direction, where 0° lies on the ground track. Positive values are to the left and negative to the right. The azimuth angle is the radiometer look angle $(\varphi_{\rm rad})$ with respect to geographic north and varies from 0° to 360°. A simplified WindSat data acquisition geometry for a descending pass is shown in Fig. 2. Even though the instrument is conically scanning, only a limited range of data in the forward and aft swaths is actually acquired. The restricted range of angles is due to issues related to instrument calibration and problems in some scan-angle ranges [16], [17].

In order to satisfy the WindSat primary mission goal of estimating the wind vector, precise measurements of all Stokes parameters are required. The order of magnitude of the U and V parameters is a few Kelvin and, therefore, a small instrument bias can result in significant contamination of these measurements. This may result in a shift in the level of the retrieved parameters. These effects are expected to be more significant near the swath edges. In order to reduce bias contamination of the geophysical signatures of the U and V parameters, we have restricted our entire analysis to scan angles between -25° and $+25^\circ$ in the forward swath. Bias associated with this scan-angle range is expected to be smaller than the rest of the scan-angle range. Published results for WindSat have shown that the 18.7-GHz measurements are the ones that are most affected by the calibration bias [16]. Hence, for this paper, we have excluded the 18.7-GHz observations.

Time series plots for each study area were developed to assist in understanding the temporal behavior of the Stokes parameters. In satellite-based studies of land, it is normally assumed that the azimuth angle has no significant effect on T_B. As a result, all footprints falling in the study area are usually averaged and compared. We expect azimuthal variations in the U and V parameters. As a result, when carrying out the temporal analysis of the U and V components for a selected study region, we also need to consider the azimuthal dependence. Therefore, we further restricted the range of analyzed scan angles from $\pm 25^\circ$ to $\pm 10^\circ$, in order to minimize the effect of azimuthal dependence. For a given latitude, the flight direction with respect to the north is fixed for all orbits; hence, restricting the scan angle also implies restricting the azimuth angle at a given latitude. This was a tradeoff between having adequate data over an area for temporal analysis and minimizing the effect of scan-angle variation within the selected angle interval. It should be noted that there might still be some residual variability associated with day-to-day variation in the mean scan angle over the area, even though we have limited the range.

Another critical point regarding the azimuth angle relates to differences between the ascending and descending passes. The selected scan-angle range for ascending and descending corresponds to different azimuth angles with respect to the north. All observations within the selected scan-angle range of -10° to $+10^\circ$ are averaged and assigned to the azimuth angle of the flight direction. This direction varies with latitude. It depends upon the WindSat orbit geometry, and ascending and descending angles are related by $\varphi_{\rm rad}$ (Ascending) $= 180^\circ - \varphi_{\rm rad}$ (Descending). For the current studies, $\varphi_{\rm rad}$ varies from 0° to 360°, and hence, the relation can be modified as $\varphi_{\rm rad}$ (Ascending) $= 540^\circ - \varphi_{\rm rad}$ (Descending). At low latitudes, the variations are small, and at high latitudes, they are large. For the selected study areas, scan angles between -10° and $+10^\circ$ correspond to average flight directions of 190° for the descending passes and 350° for the ascending passes. As part of our analysis of the land surface structural signature dependence on azimuth angle, we will examine the time series of U and V observations for both the ascending and descending orbits.

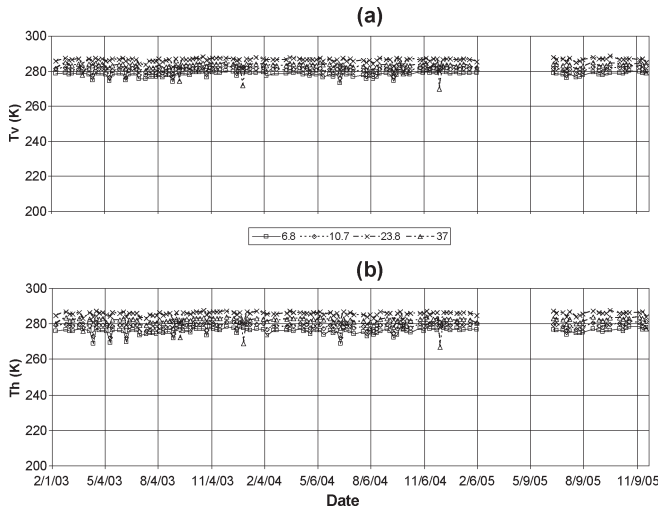

Fig. 3. WindSat brightness temperature time series for 6.8, 10.7, 18.7, and 37 GHz for (a) T_ν and (b) T_h descending observations, plotted for the period February 2003 to November 2005 for the Amazon study area in Brazil.

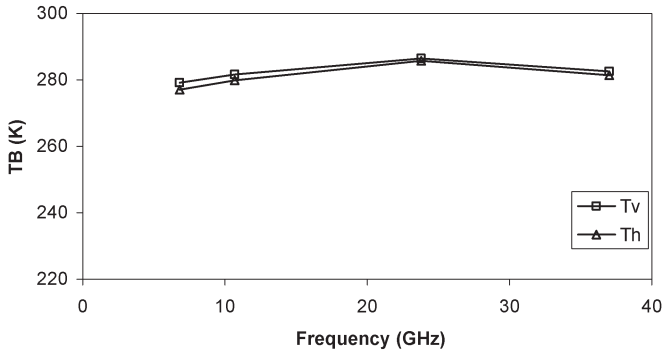

Fig. 4. Brightness temperatures at vertical and horizontal polarizations plotted as a function of frequency for the Amazon study area in Brazil. A total of 188 data points were averaged for October 2003. The standard deviation at each frequency was lower than 1.5 K.

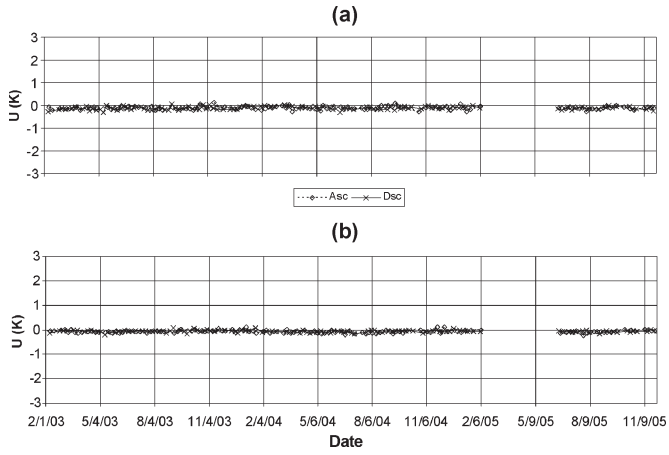

Fig. 5. Third Stokes parameters time series at (a) 10.7 GHz and (b) 37 GHz for the period of February 2003 to November 2005 for the Amazon in Brazil. The ascending ($\varphi_{\rm rad}$ averages around 190°) and descending ($\varphi_{\rm rad}$ averages around 350°) observations at each frequency are plotted together to facilitate comparison.

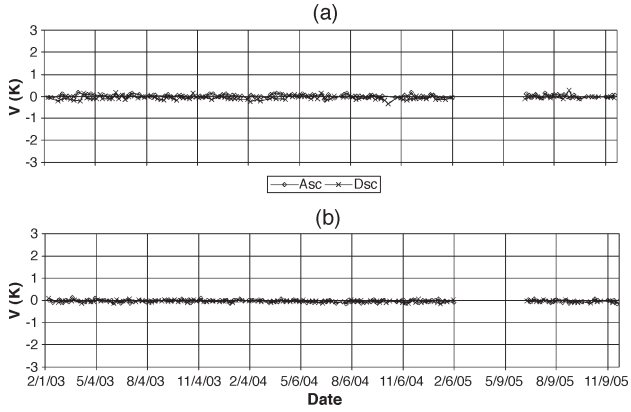

Fig. 6. Fourth Stokes parameters time series at (a) 10.7 GHz and (b) 37 GHz for the period of February 2003 to November 2005 for the Amazon in Brazil. The ascending ($\varphi_{\rm rad}$ averages around 190°) and descending ($\varphi_{\rm rad}$ averages around 350°) observations at each frequency are plotted together to facilitate comparison.

V. Data Analysis

A. Amazon Rainforest

The brightness temperature is the function of the emissivity and surface temperature of the target under investigation [3]. In the presence of vegetation, the emission from the soil surface is attenuated. In addition, vegetation adds its own radiation, which is unpolarized in nature [18]. For dense vegetation conditions such as the Amazon at WindSat frequencies, any emission from the ground surface would be masked by the canopy due to the typically high levels of vegetation opacity. Fig. 3 shows the time series of T_ν and T_h plotted for selected frequencies over an extended period. There are a few low outlier points that are likely to be associated with very large rainfall and flooding. The range of the observed brightness temperatures was found to agree with the previous investigations [19]. Fig. 4 shows the spectral plot of brightness temperature for the study area. The nearly unpolarized nature of this particular dense vegetation results in values of T_ν and T_h that are very similar at all frequencies, as expected [18]. The T_B at 37 GHz shows a small drop, which is likely due to the sensitivity of this channel to atmospheric extinction and surface scattering [12]. The long-term invariant nature of the Amazon is apparent in Fig. 3. Brightness temperature fluctuates within the same range over an extended period. This characteristic of the region makes the Amazon useful as a vicarious calibration (thermal stability) target for the instrument.

The times series of 10.7- and 37-GHz U and V for the Amazon study area are plotted in Figs. 5 and 6, respectively. The U and V parameters for an isotropic area are expected to be zero. The WindSat 10.7-GHz U and V measurements support this assumption that the area is isotropic. A small shift ($\sim$0.1 K) from zero was observed that is likely the result of an instrument bias. The absolute error in U and V is 0.25 K [1], hence, any fluctuation below this range can be considered due to instrument noise. The T_B scale in Figs. 5 and 6 was chosen to facilitate comparison with the other selected anisotropic areas. The long-term invariant U and V parameters at both the frequencies reflect the invariant nature of the Amazon; these also support the reliability of the WindSat U and V channels. Similar trends were found for the 37-GHz channel.

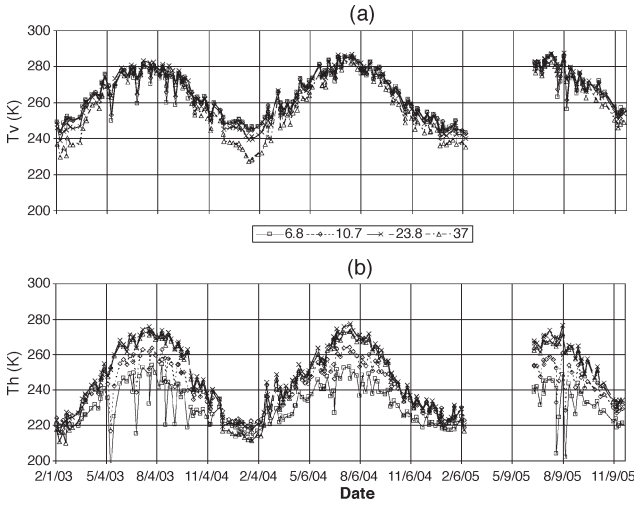

Fig. 7. WindSat measured brightness temperature time series for 6.8, 10.7, 18.7, and 37 GHz for (a) T_ν and (b) T_h descending observations plotted for the period February 2003 to November 2005 for the rangelands of Mongolia.

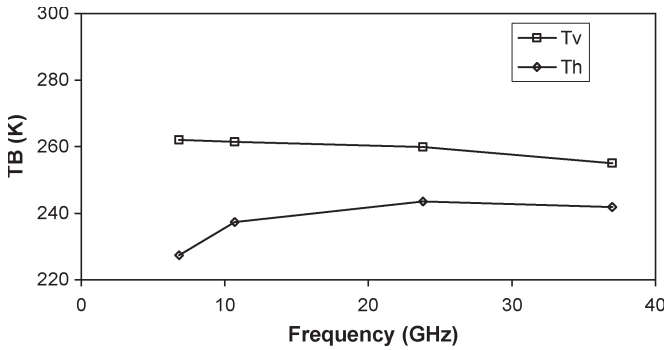

Fig. 8. Brightness temperatures at vertical and horizontal polarizations plotted as a function of the frequency for the Mongolia study area. A total of 282 data points were averaged for October 2003. The standard deviation for each frequency was smaller than 2 K.

B. Mongolia Rangeland

The selected area located in Mongolia is instrumented for *in situ* soil-moisture measurements. Jackson *et al.* [13] have investigated this area for soil-moisture retrieval using Advanced Microwave Scanning Radiometer observations. We expect the region to be isotropic, but since it is lightly vegetated, we can examine the response of U and V to temperature and soil-moisture variations.

Fig. 7 shows the time series of T_ν and T_h for selected WindSat frequencies. An annual temperature trend is apparent in this figure, with brightness temperature varying over the range of $\sim$60 K for both polarizations. Several low spikes in the observations of T_h, mostly for 6.8 and 10.7 GHz, are the result of increases in soil moisture due to the rain events. These sharp decreases are larger for T_h, which is expected for a lightly vegetated land surface.

It is generally accepted that T_ν at 37 GHz is mainly a function of surface temperature [20]. The spectral difference between 37-GHz T_ν and a lower frequency is important in snow-related studies [21]. In Fig. 7, the T_ν at 37 GHz shows a significant drop in brightness temperature, as compared to the other frequencies, during the winter months (November to February) of both 2003

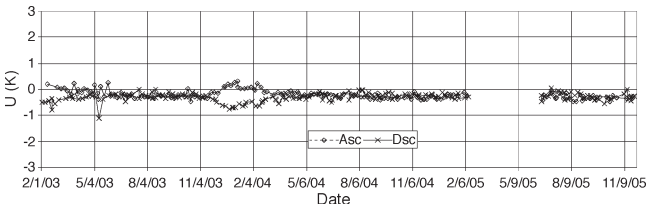

Fig. 9. Third Stokes parameters time series at 10.7 GHz for the period of February 2003 to November 2005 for the rangelands of Mongolia. The ascending ($\varphi_{\rm rad}$ averages around 190°) and descending ($\varphi_{\rm rad}$ averages around 350°) observations at each frequency are plotted together to facilitate comparison.

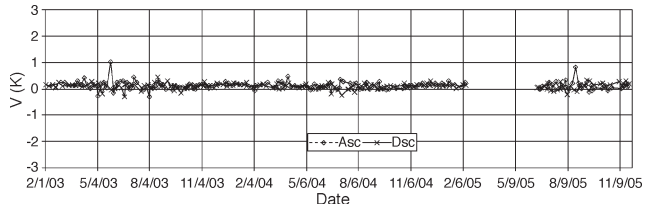

Fig. 10. Fourth Stokes parameters time series at 10.7 GHz for the period of February 2003 to November 2005 for the rangelands of Mongolia. The ascending ($\varphi_{\rm rad}$ averages around 190°) and descending ($\varphi_{\rm rad}$ averages around 350°) observations at each frequency are plotted together to facilitate comparison.

and 2004. This may be the result of the presence of snow during that period. This drop is not apparent in 2005 due to the missing data.

Fig. 8 shows the spectral plot of T_ν and T_h over the Mongolia rangeland study area. In order to produce the spectral plot, a time period must be selected to ensure an adequate sample size ($\sim$200). However, averaging highly variable conditions is not useful. Therefore, we chose the month of October 2003, when no spikes are present, in an attempt to minimize temperature variations over time. From theory [3], the dielectric constant should decrease with an increasing frequency, which should result in increasing emissivity and increasing brightness temperature. We expect T_ν to be mainly a function of temperature and T_h to be mainly a function of the dielectric constant. As a result, T_h is expected to have larger variations between the brightness temperatures at different frequencies as compared to T_ν. In addition, parameters such as penetration depth, atmospheric conditions, and surface scattering also affect this relationship. The trends in Fig. 8 are typical of bare or lightly vegetated soils [18]. The larger changes from 10- to 6-GHz h are likely to be associated with surface roughness and vegetation effects as well as a difference in the effective temperature contributing to the measurement.

As noted previously, the Mongolia area facilitates the examination of U and V responses for soils because of the low amounts of vegetation, small topographic variations, and some significant soil moisture variability. Figs. 9 and 10 show the 10.7-GHz U and V plots over the study period. Ascending and descending U observations show good agreement, except for the winter months of 2003 and 2004 (data for 2005 are missing). The 37-GHz measurements also show similar trends (not presented here), but exhibited additional variability during the 2004 winter. Based upon the T_ν and T_h analysis, it was concluded that, during the winter periods of 2003 and 2004, there might be snow cover that results in the U response and

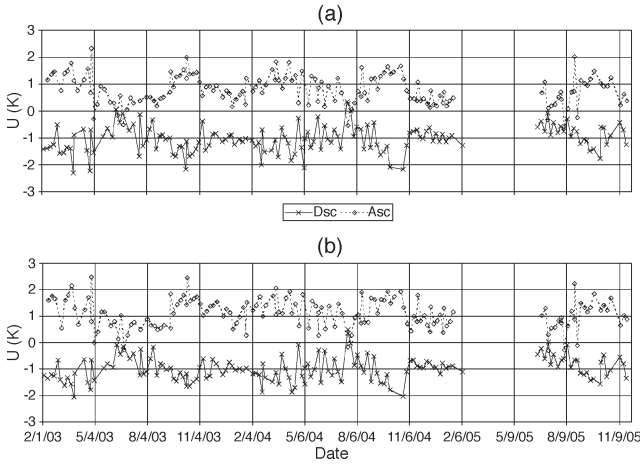

Fig. 11. Third Stokes parameters time series at (a) 10.7 GHz and (b) 37 GHz for the period of February 2003 to November 2005 for the Taklamakan Desert study area in China. The ascending ($\varphi_{\rm rad}$ averages around 190°) and descending ($\varphi_{\rm rad}$ averages around 350°) observations at each frequency are plotted together to facilitate comparison.

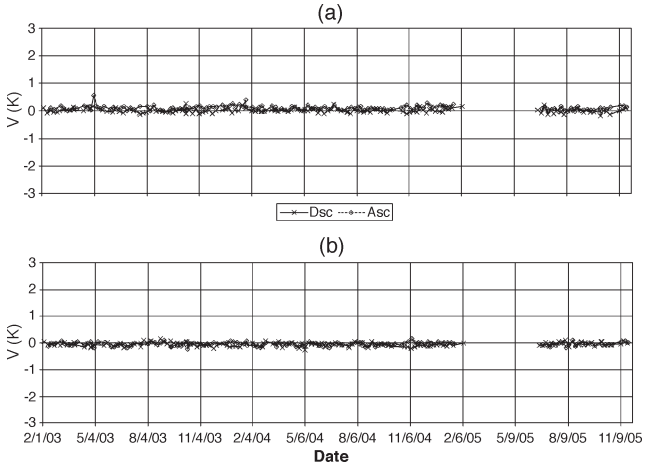

Fig. 12. Fourth Stokes parameters time series at (a) 10.7 GHz and (b) 37 GHz for the period of June 2003 to January 2005 for the Taklamakan Desert study area in China. The ascending ($\varphi_{\rm rad}$ averages around 190°) and descending ($\varphi_{\rm rad}$ averages around 350°) observations at each frequency are plotted together to facilitate comparison.

a difference between ascending and descending observations. If the winter months are excluded from the analysis, then the U and V results indicate that the region is isotropic and that soil-moisture variations (obvious in the T_ν and T_h data) do not affect U and V measurements.

C. Taklamakan Desert

The Taklamakan Desert in western China was chosen for the study of WindSat polarimetric (U and V) signals over structured bare soils. Bartalis *et al.* [14] used scatterometer observations over the Taklamakan Desert to demonstrate the importance of the scan angle over structured regions. The area consists of large sand dunes oriented northeast with their slopes facing the southeast and northwest [see Fig. 1(a)]. Sand dune orientation in a specific direction over the entire region (larger than a WindSat footprint) provides an opportunity to investigate the impact of land surface structure on the polarimetric signals. The 10.7- and 37-GHz U and V time series are shown in Figs. 11 and 12. The U observations for ascending orbits (positive T_B) are inversely related to the descending orbits (negative T_B) for both frequencies (Fig. 11). The response for the U channels are clear and consistent and indicate that surface structure at this scale can impact a satellite-sized footprint.

The selected scan-angle range corresponds to the average radiometer azimuth angles with respect to the north ($\varphi_{\rm rad}$) for the descending ($\sim 190^\circ$) and ascending passes ($\sim 350^\circ$). The large topographic structure of the Taklamakan Desert surface is analogous to large ocean waves, with the slopes of the sand dunes oriented southeast ($\sim 120^\circ$ with respect to the north) and northwest ($\sim 300^\circ$ with respect to the north). The southeast slopes are oriented along the upwind direction (in the direction of the prevailing winds), resulting in a land surface orientation angle of $\varphi_{\rm orient} \sim 120^\circ$. The relative azimuth angle $\varphi_{\rm relative}$ is the difference between the orientation of the land surface features and radiometer azimuth angle $\varphi_{\rm rad}$. The $\varphi_{\rm relative}$ was estimated to be $\sim 290^\circ \pm 8^\circ$ for the descending orbits and $\sim 130^\circ \pm 8^\circ$ for the ascending orbits. From theory and aircraft observations [7], [21], for a relative azimuth angle of 290°, the U response is expected to be positive in magnitude, and for 130°, the response is expected to be negative in magnitude. However, these observations have the opposite signs for both the ascending and descending $\varphi_{\rm relative}$ angles. This is due to the definition of the U and V for WindSat, which is off by a minus sign from the aircraft data [23] (Fig. 12). These results clearly demonstrate the presence of a structural signature in the WindSat U parameter over a structured bare soil surface.

Although we observed a response for the U parameter, no significant variation was observed in the V response in either temporal or azimuthal analyses (Fig. 12). The ascending and descending observations were found to be close to zero.

D. Heilongjiang Agriculture

The Heilongjiang agriculture area in north China was chosen to study the WindSat polarimetric response of structured vegetation. This area consists of numerous small agricultural fields with almost all the field rows oriented very close to the north–south direction. Fig. 1(b) clearly shows the regional pattern. From this image, the field structure orientation angle is estimated as $\varphi_{\rm orient} = 80^\circ$.

A previous ground-based study conducted at L-band [9] showed a dependence of the U and V parameters on vegetation rows and height. The Heilongjiang site had been identified in [14] and [15] as a target with a possible polarimetric response using backscatter coefficient data that showed a clear second harmonic dominance in the azimuth dependence.

The 10.7- and 37-GHz U time series are plotted in Fig. 13. The ascending observations lie close to 0 K, whereas the descending data have negative values during the summer months, with the maxima occurring during July of all three years. During winter, this area is predominantly bare soils, and observations during these months exhibit no response for U and V. The summer period response was larger for 10.7 GHz as compared to 37 GHz. The lower frequency of 10.7 GHz increases

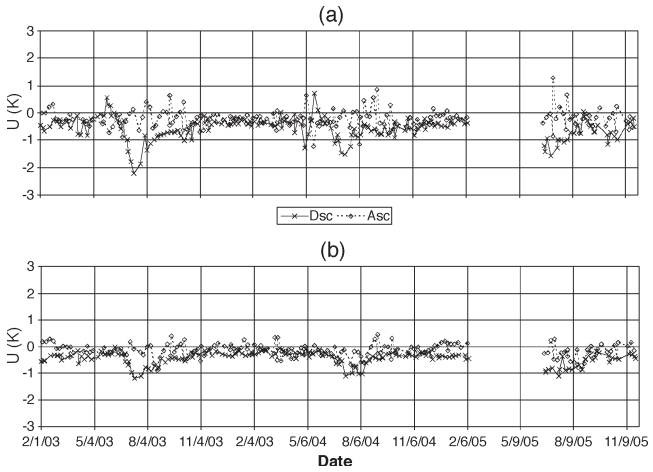

Fig. 13. Third Stokes parameters time series at (a) 10.7 GHz and (b) 37 GHz for the period of February 2003 to November 2005 for the Heilongjiang agricultural study area in eastern China. The ascending ($\varphi_{\rm rad}$ averages around 190°) and descending ($\varphi_{\rm rad}$ averages around 350°) observations at each frequency are plotted together to facilitate comparison.

the potential canopy penetration, and as a result, different components of the vegetation may contribute to the signal at different frequencies.

Because $\varphi_{\rm rad}$ for the ascending orbits is $\sim 350^\circ$ and $\sim 190^\circ$ for the descending over the Heilongjiang area, the relative azimuth angle is $\sim 90^\circ$ for the ascending and $\sim 250^\circ$ for the descending passes. Based upon results presented in [7] and [22], a relative azimuth angle of 90° should result in $U = 0$ K, and for 250°, it should be a positive value. Again, note that the definition of the U and V of WindSat is off by a minus sign from the aircraft data [23]. The ascending and descending U observations show these features, with the ascending observations fluctuating around a small negative value that we interpreted as sensor bias, which for this area was larger than that of the Amazon study area in Brazil discussed previously. This is probably the result of the variations introduced by the sun's illumination of the warm calibration load [16]. As this error varies periodically during each orbit, the bias observed for this region is not in contradiction with the small bias observed for the Amazon region (Fig. 5).

Further examination of this data was conducted by separating the available azimuth angle range of $+25^\circ$ to -25° for the ascending passes into 10° increments. Fig. 14 shows the time series for three scan-angle intervals: -25° to -15°, -5° to $+5^\circ$, and $+15^\circ$ to $+25^\circ$ (ascending orbits). These three scan-angle intervals correspond to average radiometer azimuth angles of $\sim 10^\circ$, $\sim 350^\circ$, and $\sim 330^\circ$, respectively. From the satellite image shown in Fig. 1(b), the orientation of the field rows is $\sim 350^\circ$, which is almost the same as the direction of the ascending pass. From theory, for an azimuth angle of 350°, the -45° and $+45^\circ$ polarized T_B should be similar. Any deviation from this scan-angle range is expected to produce different brightness signals in the 45° channels, resulting in a nonzero U value. Fig. 14 shows this effect very clearly. The U observations for the 350° azimuth angle (azimuth angle between 345° and 355°) fall between the observations of the 10° (azimuth angle between 5° and 15°) and the 330° azimuth angle (azimuth angle

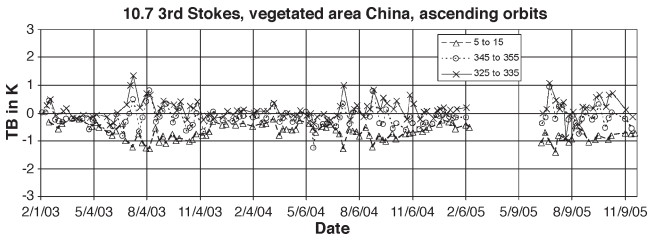

Fig. 14. WindSat 10.7-GHz third Stokes parameter three time series plotted for the scan-angle intervals between 5° and 15°, 345° and 355°, and 325° and 335° of ascending orbits for the Heilongjiang agriculture region in China.

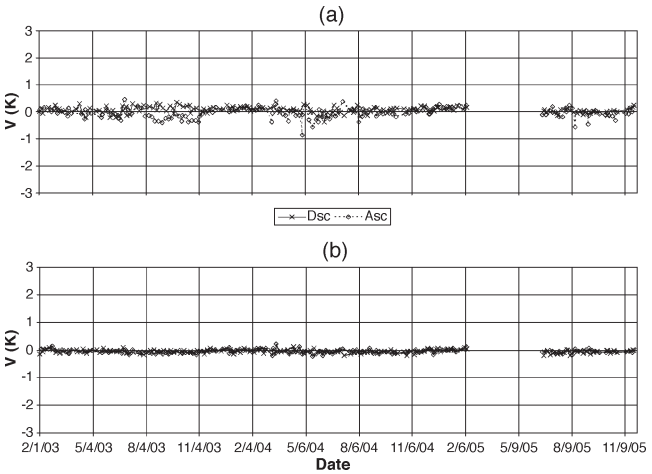

Fig. 15. Fourth Stokes parameters time series at (a) 10.7 GHz and (b) 37 GHz for the period of February 2003 to November 2005 for the Heilongjiang agricultural study area in eastern China. The ascending ($\varphi_{\rm rad}$ averages around 190°) and descending ($\varphi_{\rm rad}$ averages around 350°) observations at each frequency are plotted together to facilitate comparison.

between 325° and 335°). The relative azimuth angles for 10° and 330° are estimated to be $\sim 20^\circ$ and $\sim 340^\circ$, respectively. As per the theory, U at a relative azimuth angle of 20° should be positive, and at 340°, it should be negative. The curves of Fig. 14 agree with the theory and, therefore, demonstrate that structured vegetated conditions can produce a nonzero U signature.

The time series of the 10.7- and 37-GHz V channels for the Heilongjiang agriculture region are shown in Fig. 15. Recall that no V response was observed for the structured bare soil of the Taklamakan Desert. However, for this agricultural region, a systematic V response was observed in the 10.7-GHz observations between August and October of 2003. The V signal appears to lag the U observations. This is likely to be related to either senescence of the vegetation or harvesting. The ascending observations were negative, and the descending were positive. There is some evidence of a similar response in 2004 and 2005; however, it is not as consistent as 2003. From the study in [7], the V responses should be 180° out of phase compared to the U parameter. The WindSat V measurement shows good agreement with the theory when compared to that of the U parameter in Fig. 13.

The 37-GHz V data did not exhibit the same response as 10.7 GHz. Both the ascending and descending observations are close to zero [Fig. 15(b)]. These results suggest a possible canopy penetration effect; 37 GHz is not expected to sense as

deep into a canopy as 10 GHz. These preliminary results also clearly warrant a more rigorous analysis of the V parameter for vegetation.

VI. Conclusion

Polarimetric passive microwave measurements may provide new information that can be used to estimate or describe land surface features. Data from the WindSat instrument were used in this paper to determine if this was possible. Issues of satellite footprint size placed restrictions on the size of the study area. As a result, four large and homogenous regions were identified that represented unique land surface features.

The analysis of the Amazon rainforest data showed consistency for T_ν and T_h over a densely vegetated area. The U and V observations demonstrated the invariant isotropic nature of the region and the reliability of the sensor data. The Mongolia rangeland site was selected to represent isotropic conditions with less vegetation and time-varying temperature and soil moisture. The U and V responses over this area were very close to zero for most of the year. From this, we concluded that there was no soil-moisture effect present in the U or V measurements. The Taklamakan Desert area in China is topographically anisotropic, and this gives rise to significant responses of the U parameter to the observed dune structure. The time series of the U parameter also agreed with sea surface polarimetric theory. The U and V parameters for the Heilongjiang agriculture region showed structural dependence in the presence of agricultural crops. The trend of the U parameter was found to agree with a ground-based study made with an L-band polarimetric radiometer.

The results of this paper clearly show that there is a response in the U channel when aligned land surface features are present in the footprint. This is the first time this has been observed at satellite footprint scales. Further controlled condition studies of vegetation features are needed to refine our understanding. How to use this new information in application, such as soil-moisture retrieval, is the next challenge.

References

[1] P. W. Gaiser, K. M. St. Germain, E. M. Twarog, G. A. Poe, W. Purdy, D. Richardson, W. Grossman, W. L. Jones, D. Spencer, G. Golba, J. Cleveland, L. Choy, R. M. Bevilacqua, and P. S. Chang, "The WindSat spaceborne polarimetric microwave radiometer: Sensor description and early orbit performance," *IEEE Trans. Geosci. Remote Sens.*, vol. 42, no. 11, pp. 2347–2361, Nov. 2004.

[2] L. Tsang, J. A. Kong, and R. T. Shin, *Theory of Microwave Remote Sensing*. New York: Wiley, 1985.

[3] F. T. Ulaby, R. K. Moore, and A. K. Fung, *Microwave Remote Sensing, Active and Passive*, vol. 3. Norwood, MA: Artech House, 1986.

[4] H. Stephen and D. G. Long, "Modeling microwave emissions of erg surfaces in the Sahara Desert," *IEEE Trans. Geosci. Remote Sens.*, vol. 43, no. 12, pp. 2822–2830, Dec. 2005.

[5] T. Meissner and F. Wentz, "An updated analysis of the ocean surface wind direction signal in passive microwave brightness temperatures," *IEEE Trans. Geosci. Remote Sens.*, vol. 40, no. 6, pp. 1230–1240, Jun. 2002.

[6] L. Tsang, "Polarimetric passive remote sensing of random discrete scatterers and rough surfaces," *J. Electromagn. Waves Appl.*, vol. 5, no. 1, pp. 41–57, 1991.

[7] S. H. Yueh, "Modeling of wind direction signals in polarimetric sea surface brightness temperatures," *IEEE Trans. Geosci. Remote Sens.*, vol. 35, no. 6, pp. 1400–1418, Nov. 1997.

[8] S. H. Yueh, R. Kwok, F. K. Li, S. V. Nghiem, W. J. Wilson, and J. A. Kong, "Polarimetric passive remote sensing of ocean wind vector," *Radio Sci.*, vol. 29, no. 4, pp. 799–814, Jul./Aug. 1994.

[9] S. Sobjaerg and N. Skou, "Polarimetric signature from crop covered land surface measured by an L-band polarimetric radiometer," in *Proc. IGRASS*, Toulouse, France, Jul. 2003, pp. 2626–2628.

[10] H. Pham, E. J. Kim, and A. W. England, "A calibration approach for microwave polarimetric radiometer," *IEEE Trans. Geosci. Remote Sens.*, vol. 43, no. 11, pp. 2443–2451, Nov. 2005.

[11] S. V. Nghiem, M. E. Veysoglu, R. T. Shin, J. A. Kong, K. O'Neill, and A. Lohanick, "Polarimetric passive remote sensing of a periodic soil surface: Microwave measurements and analysis," *J. Electromagn. Waves Appl.*, vol. 5, no. 9, pp. 997–1005, 1991.

[12] E. Njoku, T. Chan, W. Crosson, and A. Limaye, "Evaluation of the AMSR-E data calibration over land," *Ital. J. Remote Sens.*, vol. 29, no. 4, pp. 19–37, 2004.

[13] T. J. Jackson, R. Hurkmans, A. Hsu, and M. Cosh, "Soil moisture algorithm using data from the Advanced Microwave Scanning Radiometer (AMSR-E) in Mongolia," *Ital. J. Remote Sens.*, vol. 30, no. 31, pp. 23–32, 2004.

[14] Z. Bartalis, K. Scipal, and W. Wagner, "Azimuthal signature of scatterometer measurements over different land cover types in China," in *Proc. Conf. ISPMSRS*, Beijing, China, Oct. 2005, pp. 24–26.

[15] Z. Bartalis, K. Scipal, and W. Wagner, "Azimuthal anisotropy of scatterometer measurements over land," *IEEE Trans. Geosci. Remote Sens.*, vol. 44, no. 8, pp. 2083–2092, Aug. 2006.

[16] E. M. Twarog, W. E. Purdy, P. W. Gaiser, K. H. Cheung, and B. E. Kerlm, "WindSat on-orbit warm load calibration," *IEEE Trans. Geosci. Remote Sens.*, vol. 44, no. 3, pp. 516–529, Mar. 2006.

[17] W. L. Jones, J. D. Park, S. Soisuvarn, L. Hong, P. W. Gaiser, and K. M. St. Germain, "Deep-space calibration of the WindSat radiometer," *IEEE Trans. Geosci. Remote Sens.*, vol. 44, no. 3, pp. 476–495, Mar. 2006.

[18] T. J. Jackson, R. Bindlish, A. Gasiewski, B. Stankov, M. Klein, E. Njoku, D. Bosch, T. Coleman, C. Laymon, and P. Starks, "Polarimetric scanning radiometer C- and X-band microwave observations during SMEX03," *IEEE Trans. Geosci. Remote Sens.*, vol. 43, no. 11, pp. 2418–2430, Nov. 2005.

[19] J. Calvet, J. Wigneron, E. Mougin, Y. H. Kerr, and J. L. S. Brito, "Plant water content and temperature of the Amazon forest from satellite microwave radiometry," *IEEE Trans. Geosci. Remote Sens.*, vol. 32, no. 2, pp. 397–408, Mar. 1994.

[20] R. A. M. De Jeu, "Retrieval of land surface parameters using passive microwave remote sensing," Ph.D. dissertation, Faculty Earth Science, Vrije Univ., Amsterdam, The Netherlands, 2003.

[21] A. K. Fung, *Microwave Scattering and Emission Models and Their Applications*. Norwood, MA: Artech House, 1994.

[22] S. H. Yueh, W. J. Wilson, S. J. Dinardo, and S. V. Hsiao, "Polarimetric microwave wind radiometer model function and retrieval testing for WindSat," *IEEE Trans. Geosci. Remote Sens.*, vol. 44, no. 3, pp. 584–596, Mar. 2006.

[23] S. H. Yueh, R. Kwok, and S. V. Nghiem, "Polarimetric scattering and emission properties of targets with reflection symmetry," *Radio Sci.*, vol. 29, no. 6, pp. 1409–1420, Nov./Dec. 1994.

Parag S. Narvekar received the M.Sc. degree in physics from Goa University, Taleigao Plateau, Goa, India, in 2001. He is currently working toward the Ph.D. degree in passive polarimetric microwave remote sensing at the University of Bremen, Bremen, Germany.

He worked as a Research Associate with the Microwave Remote Sensing Laboratory, Indian Institute of Technology (IIT) Bombay, from 2001 to 2004. His work there included data processing, SAR interferometry for digital elevation model (DEM) generation and surface deformation studies, analysis of passive microwave data from multifrequency scanning microwave radiometer (MSMR) flown onboard IRS-P4 and its calibration/validation, and application of electromagnetic models for geophysical parameter retrievals. He is currently with the Hydrology and Remote Sensing Laboratory, U.S. Department of Agriculture, Beltsville, MD, as a Visiting Scientist. His current research interest includes passive polarimetry for land surfaces, scatterometers, and electromagnetic modeling.

Thomas J. Jackson (SM'96–F'02) received the Ph.D. degree from the University of Maryland, College Park, in 1976.

He is currently a Research Hydrologist with the U.S. Department of Agriculture, Agricultural Research Service (ARS), Hydrology and Remote Sensing Laboratory, Beltsville, MD. He joined ARS in 1977. His research involves the application and development of remote-sensing technology in hydrology and agriculture, primarily microwave measurement of soil moisture. He is or has been a member of the science and validation teams of the Aqua, ADEOS-II, Radarsat, Oceansat-1, Envisat, ALOS, SMOS, and Hydros remote-sensing satellites.

Dr. Jackson is a Fellow of the American Meteorological Society and American Geophysical Union. In 2003, was the recipient of the AGU Hydrology Award and the NASA/Department of Interior William T. Pecora Award. He is a member of the IEEE Geoscience and Remote Sensing (GRSS) Administrative Committee, serving as its Secretary. He was recognized by the IEEE GRSS with its Outstanding Service Award in 2002.

Rajat Bindlish (M'00–SM'05) received the B.S. degree from the Indian Institute of Technology, Bombay, in 1993, and the M.S. and Ph.D. degrees from Pennsylvania State University, University Park, in 1996 and 2000, respectively, all in civil engineering.

He is currently with SSAI, Inc., working at the U.S. Department of Agriculture, Agricultural Research Service, Hydrology and Remote Sensing Laboratory, Beltsville, MD. His research interests involve the application of microwave remote sensing in hydrology. He is currently working on soil-moisture estimation from microwave sensors and their subsequent application in land surface hydrology.

Li Li (M'96–SM'06) received the M.S. degree from the Beijing University of Posts and Telecommunications, Beijing, China, in 1987 and the Ph.D. degree from the University of Washington, Seattle, in 1995, both in electrical engineering.

He is currently with the Naval Research Laboratory (NRL), Washington, DC, working on spaceborne radiometry of land and ocean surfaces, particularly for the applications of the NRL WindSat and NPOESS microwave imager sensors. From 1997 to 2004, he was a Senior Scientist at the Jet Propulsion Laboratory (JPL), California Institute of Technology, where he participated in several NASA projects, including the Aqua Advanced Microwave Scanning Radiometer (AMSR-E), CloudSat Cloud Profiling Radar (CPR), and the JPL second-generation precipitation radar. He was a Student Visitor during 1993–1995 at the National Center for Atmospheric Research, Boulder, CO. From 1995 to 1997, he was with the Caelum Research Corporation, working at the Office of Research and Application, National Environmental Satellite, Data, and Information Service, National Oceanic and Atmospheric Administration, Camp Springs, MD.

Dr. Li is a member of the American Geophysical Union and Eta Kappa Nu. He is the recipient of the National Center for Atmospheric Research/Research Applications Program Fellowship 1993–1995, NASA Group Achievement Awards, and the JPL Technical Excellence Award in 2002.

Georg Heygster (M'00) was born in Braunschweig, Germany, in 1951. He received the Diploma degree in solid-state physics and the Ph.D. degree in image processing from the University of Göttingen, Göttingen, Germany, in 1976 and 1979, respectively.

He was a Consultant with the Computer Center of the University of Bremen, Germany, from 1979 to 1988. Since then, after one year in the field of imaging mechanisms of the scanning acoustic microscope, he has been the head of the group Physical Analysis of Remote Sensing images (PHAROS), Institute of Environmental Physics, University of Bremen, Bremen, Germany. His research activities include passive and active microwave remote sensing, especially of both surface and atmosphere of the high latitudes.

Peter Gaiser (S'91–M'93–SM'04) received a B.S. degree in Electrical Engineering from Virginia Polytechnic Institute and State University, Blacksburg, in 1987, and Ph.D. degree from the University of Massachusetts at Amherst, in 1993, where he studied microwave remote sensing, with emphasis on synthetic aperture interferometric radiometry.

He has been with the Naval Research Laboratory (NRL), Washington, DC, since 1993, and is currently the Head of the Remote Sensing Physics Branch, Remote Sensing Division, NRL. While at NRL, he has been involved in a variety of microwave and millimeter-wave radiometry projects, with a concentration on polarimetric radiometry research. His research interests include instrument design, development, and calibration, data collection, and model development specifically for the purpose of ocean wind vector measurements from space. He is the Principal Investigator for the WindSat spaceborne polarimetric microwave radiometer demonstration project.